Geophysical Research Letters

RESEARCH LETTER
10.1029/2019GL086625

A Mixed Length Scale Model for Migrating Fluvial Bedforms

M. Guala[1,2], M. Heisel[1,2], A. Singh[3], M. Musa[4], D. Buscombe[5], and P. Grams[6]

[1]St. Anthony Falls Laboratory, University of Minnesota, Minneapolis, MN, USA, [2]Civil, Environmental and Geological Engineering, University of Minnesota, Minneapolis, MN, USA, [3]Civil, Environmental and Construction Engineering, University of Central Florida, Orlando, FL, USA, [4]Environmental Science Division, Oak Ridge National Laboratory, Oak Ridge, TN, USA, [5]School of Earth and Sustainability, Northern Arizona University, Flagstaff, AZ, USA, [6]U.S. Geological Survey, Southwest Biological Science Center, Grand Canyon Monitoring and Research Center, Flagstaff, AZ, USA

Key Points:
- Scale-dependent bedform migration velocities are confirmed using laboratory and field measurements
- Bedform velocity depends on stream depth, sediment diameter and shear velocity, reorganized into frictional and bankfull scaling parameters
- A mixed length scale is proposed in a simplified predictive model

Correspondence to:
M. Guala,
mguala@umn.edu

Citation:
Guala, M., Heisel, M., Singh, A., Musa, M., Buscombe, D., & Grams, P. (2020). A mixed length scale model for migrating fluvial bedforms. *Geophysical Research Letters*, *47*, 2019GL086625. https://doi.org/10.1029/2019GL086625

Received 16 DEC 2019
Accepted 6 MAY 2020
Accepted article online 24 MAY 2020

Abstract With the expansion of hydropower, in-stream converters, flood-protection infrastructures, and growing concerns on deltas fragile ecosystems, there is a pressing need to evaluate and monitor bedform sediment mass flux. It is critical to estimate real-time bedform size and migration velocity and provide a theoretical framework to convert easily accessible time histories of bed elevations into spatially evolving patterns. We collected spatiotemporally resolved bathymetries from laboratory flumes and the Colorado River in statistically steady, homogeneous, subcritical flow conditions. Wave number and frequency spectra of bed elevations show compelling evidence of scale-dependent velocity for the hierarchy of migrating bedforms observed in the laboratory and field. New scaling laws were applied to describe the full range of migration velocities as function of two dimensionless groups based on the bed shear velocity, sediment diameter, and water depth. Further simplification resulted in a mixed length scale model estimating scale-dependent migration velocities, without requiring bedform classification or identification.

Plain Language Summary Sand and gravel sediment in river beds often forms wave-like patterns called ripples or dunes, which are collectively referred to as bedforms. The flow of the river causes bedforms to form and slowly travel downstream, thus contributing to sediment transport, erosion, and deposition along the river and to the evolution of deltas. Predicting how fast bedforms move can improve our ability to estimate sediment load carried by rivers. In this study, experimental measurements of bedforms in a laboratory facility and in the Colorado River are used to better understand bedform movement. This study confirms that smaller bedforms move faster than larger bedforms and provides a simple equation to predict the speed of moving bedforms of different sizes based on the bedform length, the size of the sediment grains, and the depth of the river.

1. Introduction

Accurate estimates of bedform and sediment mass flux are critical to understanding the evolution of fluvial, estuarine, and deltaic ecosystems, as well as to designing next-generation hydropower systems. Just within the latter example, hydropower generates roughly 16% of the worlds electricity (IEA, 2017), and it is expanding to low head energy systems. The U.S. Department of Energy is currently investing to ensure that sediment continuity can be enforced to minimize the ecological impact of the dams and of the related sediment flushing operations (Witt et al., 2017). Uncertainties in suspended sediment loads and bedform mass flux estimates are a barrier for the development of next-generation sustainable hydropower and more generally for the definition of boundary conditions and controls in geomorphic systems.

Currently, practices for estimating bedform mass flux rely on in situ measurements from sediment traps or a comparison between sequential three-dimensional bathymetric profiles (Shelley et al., 2013). In the absence of monitoring stations providing these measurements, predictive models are used for the bedform migration velocities. These models traditionally assume the representative bedform is rigidly translated at a constant velocity (Simons et al., 1965). Bedform dynamics are highly nonlinear and complex, making it difficult to predict bedform geometry, kinematics, and contribution to sediment transport (Best, 2005; Bradley & Venditti, 2019; Coleman & Nikora. 2009; Keylock et al., 2014; Martin & Jerolmack, 2011; McElroy & Mohrig, 2009; Venditti et al., 2005). However, in uniform flows, fluvial bedforms exhibit self-similar

properties across a range of spatiotemporal scales. These properties are manifested in the power law scaling regime of bed elevation spectra, which persists under different hydraulic, hydrologic, and geomorphic conditions (Aberle & Nikora, 2006; Ganti et al., 2011; Khosronejad & Sotiropoulos, 2014; Nikora & Goring, 2001; Passalacqua et al., 2006; Pelletier, 1999; Singh et al., 2010, 2011).

Since the early work of Hino (1968) and Nikora et al. (1997) on migrating fluvial bedforms, it has been argued that a constant convection velocity cannot be used in the conversion between spatial and temporal bed elevations. This implies that bedform wavelength (λ) and period (T) are not necessarily linearly substitutable, and that measuring fluvial bed elevation along a longitudinal transect x, $z(x)$, or at a specific location over time t, $z(t)$, is not equivalent. The most robust experimental evidence comes from frequency (ω) and wavenumber (k) bed elevation spectra, which do not exhibit the same power law scaling exponents when computed on $z(x)$ or $z(t)$ data sets (Guala et al., 2014; Hino, 1968; Nikora et al., 1997). Such a mismatch demonstrates that a scale-dependent, as opposed to constant, bedform convection velocity, $U_b(k)$, is required to satisfy both scaling regimes. In other words, different size bedforms predominantly migrate at different velocities. As such, a single velocity value (i.e., the equivalent of Taylor's "frozen turbulence" hypothesis commonly used in boundary layer turbulence) is not applicable for migrating bedforms. Forcing the scale dependency through $U_b(k) = \omega/k \sim k^{\beta}$, with $\beta > 0$ denoting a slower convection velocity for larger size bedforms, is equivalent to imposing a relationship between frequency and wavenumber. As a consequence, the three scaling exponents governing (1) the wavenumber surface elevation spectra $\Phi_k(k) \sim k^{-\alpha}$, (2) the frequency surface elevation spectra $\Phi_\omega(\omega)\omega^{-\gamma}$, and (3) the scale-dependent convection velocity $U_b(k) \sim k^{\beta}$ are all related: $\gamma = \dfrac{\alpha + \beta}{\beta + 1}$ (Guala et al., 2014).

A direct estimate of scale-dependent convection velocity was provided by Guala et al. (2014) using continuously monitored streamwise transects, $z = z(x, t)$, to estimate the 2-D spatiotemporal power spectrum of bed surface elevations, $\Phi_{k,\omega}$, via 2-D Fourier decomposition. The method was introduced by Erm and Joubert (1991) and then employed by Krogstad et al. (1998) and LeHew et al. (2011) on velocity data in a turbulent boundary layer flow. In Guala et al. (2014), the $\Phi_{k,\omega}$ spectra were approximated by a power law functional relation between the wavelength and the period, that is, $\lambda = BT^n$. The exponent n~0.5 was observed to be fairly constant and significantly different from the value $n = 1$, which would be required for the convective velocity of bedforms to be scale invariant and thus equivalent to the translation of a frozen bathymetry. Assuming $n = 1/2$, the dimensional coefficient B was decomposed as $B = C(u_\tau d_s)^{1/2}$ as a function of two physically meaningful and readily estimated scales, that is, the shear velocity u_τ and the mean sediment diameter d_s. Those scales are broadly used in sediment transport, for example, in the theoretical formulation of particle incipient motion, in the estimates of bedload mass flux, and are employed in the 1-D bed elevation spectra normalization (Guala et al., 2014). The resulting parameterization led to a more elegant formulation of the functional dependencies between the period and wavelength:

$$\frac{\lambda}{d_s} = C\left(\frac{T,\, u_\tau}{d_s}\right)^n. \tag{1}$$

Based on the set of laboratory experiments presented in Guala et al. (2014), the fitted values $C = 2$, $n = 0.5$ were approximated as constants, with the acknowledgment that more experiments would be needed to expand the hydraulic conditions and parameter range beyond the limited range of depths and grain sizes tested.

In this contribution, we introduce new spatiotemporal resolved bed elevation data sets from the Main Channel of the St. Anthony Falls Laboratory (SAFL) and from the Colorado River (USA). The main motivation is to understand if the variability in bedform velocity, across a wide range of hydraulic conditions, can be solely described by frictional quantities, such as the shear velocity u_τ and d_s contributing to Equation 1. By following a conceptual analogy with rough wall boundary layers, we investigate whether an outer scale quantity, such as the river depth, is required for a universal model of bedform's scale-dependent velocities in sand bedded channels. We use here new measurements to validate Equation 1 across a wide enough parameter space, extending from laboratory to field scale conditions, to revisit the relevant scaling parameters and the estimates of C and n.

Table 1
Average Parameters for the Bed Elevation Data sets: Representative Sediment Grain Size d_s, Bed Shear Velocity u_τ, and Channel Depth h

Data set	d_s (mm)	u_τ ($m\,s^{-1}$)	Symbol h (m)	Source
Tilting Bed Flume, sand	0.8	0.044	0.40	Guala et al. (2014)
Tilting Bed Flume, gravel 1	1.8	0.053	0.20	Guala et al. (2014)
Tilting Bed Flume, gravel 2	1.8	0.062	0.21	Guala et al. (2014)
Main Channel	0.42	0.045	0.64	Musa et al. (2018)
Colorado River 1	0.4	0.045	9.2	Leary and Buscombe (2020)
Colorado River 2	0.27	0.070	9.6	Leary and Buscombe (2020)

[a]*Note*. The symbols are used to indicate each data set in the later figures.

2. Experimental Setup

The first laboratory-scale facility utilized for this study is the Tilting Bed Flume at the SAFL. The flume is 0.9 m wide and 18 m long and is equipped with a sediment recirculation system. The data acquisition system included a submerged sonar mounted to a computer-controlled cart. The sonar measured bed elevation, z, along a 5 m longitudinal transect with spatial resolution $\Delta x = 0.01$ m and temporal resolution $\Delta t = 13$–20 s, depending on the case. Three data sets from Guala et al. (2014) obtained in the Tilting Bed Flume are presented here: one case with sand ripples and two cases with gravel sediment forming dunes at different discharges. The Tilting Bed Flume data were reanalyzed for the current study to ensure consistent processing with the remaining data sets.

The second facility is the SAFL Main Channel, which is one of the largest flumes used for sedimentation research (Marr et al., 2010; Singh et al., 2009, 2013; Wilcock et al., 2008). The main channel is considered here to be an intermediate laboratory/field-scale facility because the size (2.75 m wide and 85 m total length) and maximum discharge (8.5 $m^3\,s^{-1}$) are comparable to small streams. The Main Channel bedforms were monitored using a submersible laser scanning device which captured instantaneous bed elevation along a 0.4 m spanwise (y) transect. The laser was mounted to a computer-controlled cart which moved longitudinally along the channel, triggering measurements in streamwise (x) intervals of $\Delta x = 0.005$ m. The measurements were repeated in time with resolution $\Delta t = 72$ s to acquire the full bed elevation signal $z(x, y, t)$. The measurements presented here are for a 7 m long section in the middle of the channel monitored for approximately 10 hr. These data, previously used as baseline reference conditions for a hydrokinetic turbine study, are described in more detail in the supplementary material of Musa et al. (2018).

The field-scale data were acquired in a relatively straight reach of the Colorado River above Diamond Creek in Arizona (USA). A specialized survey boat was used to acquire measurements including accurate geopositioning from a robotic range-azimuth system. The bed elevation at each position was measured using a 400 kHz Reson 7125 multibeam echosounder system. Similar to the Main Channel data acquisition cart, the boat moved to a series of y and x positions, then repeated the measurements in time to estimate the full bed elevation $z(x, y, t)$. The resolutions for the field measurements were $\Delta x = 0.25$ m and $\Delta t = 500$–550 s. The two field data sets analyzed for the present study were sampled in March (Colorado River 1) and July (Colorado River 2) of 2015, respectively. The March survey was conducted over a 10-hr period when the discharge was between 342 and 380 $m^3\,s^{-1}$; the July survey was conducted over a 12-hr period when discharge was between 489 and 589 $m^3\,s^{-1}$. Additional information on the survey boat and field data acquisition is provided in Kaplinski et al. (2014), Leary and Buscombe (2020), and Ashley et al. (2020). The average parameters for the data sets described above are summarized in Table 1. The representative grain size, d_s, was the median sediment diameter based on in situ sampling. The average channel depth, h, was calculated from the difference in the measured surface and bed elevations. For the laboratory-scale data sets, the water surface elevation measurements were used to determine the average water surface slope, S, for estimating the shear velocity as $u_\tau = \sqrt{gRS}$. This estimate results from the momentum balance for uniform flow conditions, where g is gravitational acceleration and R is the hydraulic radius.

For the Colorado River field data sets, the estimate of the water surface slope and the assessment of uniform flow conditions were characterized by significant uncertainties. Therefore, the shear velocity was instead

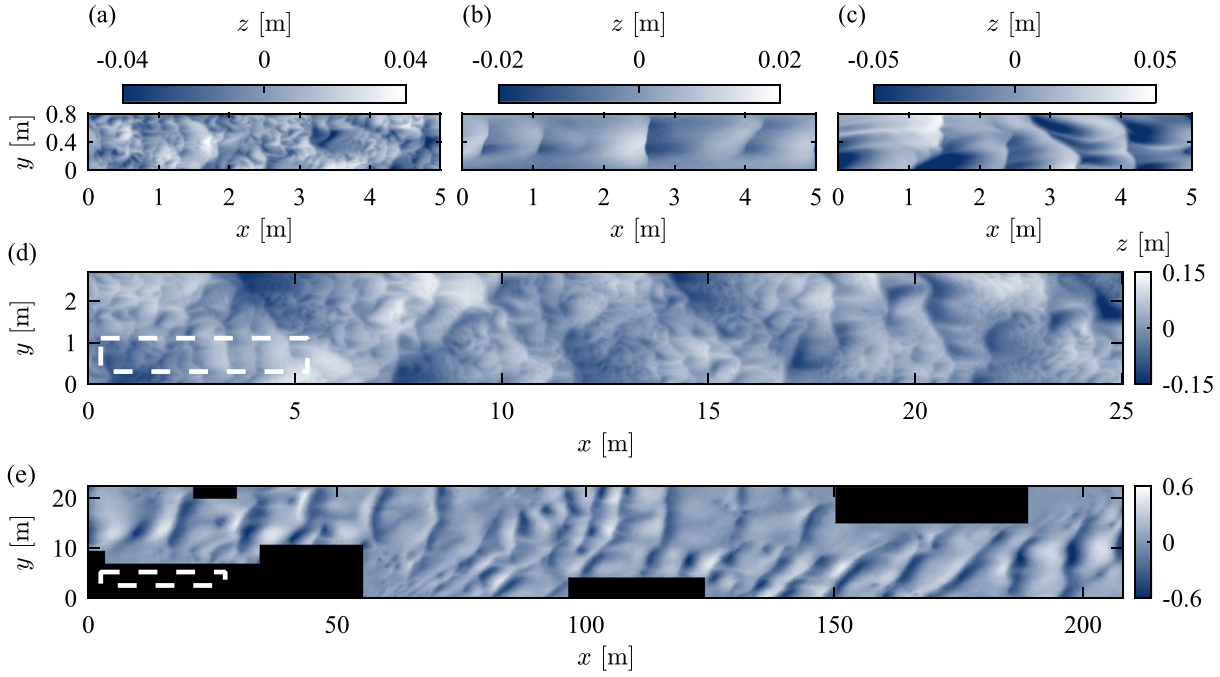

Figure 1. Sample instantaneous detrended bed elevation z (m) for the three experimental facilities: (a–c) Tilting Bed Flume at different discharges 80, 115, 135 (ls^{-1}) and bed material composition from Guala et al. (2014); (d) Main Channel baseline (Musa et al., 2018); (e) Colorado River field (Leary & Buscombe, 2020); black areas denote portion of the data set where the bathymetry was not used in the spectra computation due to errors or nonerodible features. For comparative reference, the dashed boxes in d (e) is equal in dimension to the entire measurement domains of a–c (d).

estimated using velocity measurements from a Teledyne Rio Grande Acoustic Doppler Current Profiler (ADCP). The mean velocity profile was fitted here with the logarithmic law using an aerodynamic roughness length proportional to the mean bedform height; the maximum value of $<-u'w'>$, where u' and w' are the measured streamwise and vertical velocity fluctuations, is assumed to capture a significant portion (70–80%) of the true Reynolds shear stress $\approx u_\tau^2$, while satisfying canonical rough wall scaling of the streamwise and wall normal velocity variance.

Due to the unique aspects of the experimental facilities and measurement systems, the present study is able to investigate the scaling behavior of bedform migration across a very wide parameter space. The data sets cover more than an order of magnitude range in channel depth h and bedform size (e.g., wavelength λ), and a factor five range in the shear velocity u_τ and sediment size d_s. Snapshots of bed elevation $z(x, y)$ for the Tilting Bed Flume, Main Channel facility, and the 160 m long reach of the Colorado River are included in Figure 1.

3. Data Processing

Prior to spectral analysis, each data set was detrended in space by subtracting the mean slope (i.e., the best linear fit to the elevation data), and in time by subtracting a time-averaged mean. The field measurements were characterized by occasional nonuniform intervals in the time series. The bed elevation signal was thus resampled in time using linear interpolation to achieve a uniform Δt with the same number of points as the original time series. The time intervals were shorter than the bedform time scales by an order of magnitude, and thus, the interpolation did not affect the scale-dependent results.

Bed elevation power spectra Φ were estimated using the fast Fourier transform method on the detrended signals. Streamwise segments, $z(x)$, were used to estimate spatial spectra, Φ_k, as a function of the longitudinal wavenumber, k_x (or wavelength $\lambda = k_x^{-1}$), time segments, $z(t)$, were used to estimate temporal spectra, Φ_f, as a function of the frequency, f (or period $T = f^{-1}$), and two-dimensional segments, $z(x, t)$, were used to estimate spatiotemporal spectra $\Phi(\lambda, T)$.

Conceptually, $\Phi(\lambda, T)$ provides information about the wavelength and period of bed elevation fluctuations responsible for the overall bathymetry variance. The amplitude Φ corresponds indirectly to the bedform amplitude, where the integral of Φ is the bed elevation variance σ_z^2. Because bedforms loosely resemble the sinusoidal basis functions of the Fourier transform, peaks in $\Phi(\lambda,T)$ phase space indicate a statistically dominant presence of bedforms with wavelength λ and period T. Similarly, a region of high $\Phi(\lambda,T)$ values defines the range of both wavelength and period represented by the coexisting, multiscale bedforms, which are most responsible for the variability in bed elevation. The convective velocity of these migrating bedforms can be determined as the phase velocity $U_b = \lambda/T$ at any (λ,T) point within the region of high $\Phi(\lambda,T)$. Note that the Fourier transform introduces some noise at high wavenumbers and frequencies due to the imperfect decomposition of triangular bedforms into the Fourier sinusoids.

4. Results

Figure 2a shows the spatiotemporal bed elevation spectrum, $\Phi(\lambda,T)$, for the Colorado River 2 (July 2015) data set. The spectrum is premultiplied by the wavenumber and frequency in order to emphasize trends for smaller scale bedforms; premultiplying the spectra does not affect the conclusions of the analysis. The black line in Figure 2a is a contour at 5% of the maximum Φ. The contour captures the peak of the spectrum and therefore encloses the $\lambda-T$ region corresponding to the statistically dominant bedforms. Figure 2b shows the same contour as Figure 2a and additionally includes contours for the other data sets, which show a similar shape. Across all the experiments, the premultiplied spectra identify bedforms ranging in size from $\lambda\sim$0.1 to 10 m and $T\sim$100 to 10,000 s.

The inclusion of the new Main Channel and Colorado River results in Figure 2b were used to reassess the power law exponent ($n = 0.5$) for Equation 1, which was estimated using only the laboratory-scale Tilting Bed Flume experiments (Guala et al., 2014). The exponent n is indicated by the slope of the contour region in the log-scale plots of Figures 2b, 2c, and 2e. After including the new data sets, $n = 0.6$ was found to provide a better fit to the slopes of all the spatiotemporal spectra. This change is supported by the one-dimensional spectra shown in Figure 3. Average bed elevation amplitude varies with wavenumber and frequency according to the power law exponents -3 and -2.2, respectively, observed in the 1-D spectra of Figure 3. The -3 slope is consistent with Guala et al. (2014), and the -2.2 slope is slightly steeper than the -2 value reported in Guala et al. (2014). This difference leads mathematically to the change in the scaling exponent n from 0.5 to 0.6.

In addition to the updated n value, the normalization of Equation 1 was also reassessed. Figure 2c shows the two-dimensional spectral contours normalized by the frictional scaling parameters u_τ and d_s commonly used in sediment transport models. It is apparent from Figure 2c that the frictional scaling parameters do not fully describe the variability of bedform wavelength and period across the data sets. Specifically, λ and T both increase with the increasing depth h of the Main Channel and Colorado River, as compared to the Tilting Bed Flume. The theoretical implication is that λ and T grow with the depth or width of the channel. In other words, channel geometry exerts a confinement effect which limits the bedform evolution. Because the present study focuses on streamwise-propagating bedforms, the channel geometry effects on the bedforms are most likely governed by the flow depth, h, as opposed to the channel width (e.g., for dunes, Bradley & Venditti, 2017; Colombini & Stocchino, 2012; Southard, 1991; Venditti et al., 2005). Note that the width may be increasingly relevant for more complex, three-dimensional bedforms and stream configurations (see, e.g., alternate bars and meandering onset in Seminara, 2010).

While h constrains the size of the largest bedforms, the smallest bedform size is based on self-organization of the smallest scale unit (i.e., the sediment grain size d_s). To extend the frictional scaling associated with the grain size roughness, and represent the effect of channel depth on the bedforms, the constant in Equation 1 can be relaxed to the form $C = C_1(h/d_s)^m$, where C_1 and m need to be determined.

By introducing the correction factor $(h/d_s)^m$ into Equation 1, the influence of h can be accounted for while also decreasing d_s by the same amount to ensure the relationship remains dimensionless. The exponent m determines the ratio of the outer scaling h and frictional scaling d_s in what becomes the mixed length scale. Owing to the fact that the balance between h and d_s in the normalization is unknown, the exponent m is fitted to the data rather than prescribed. By fitting the absolute maxima of $\Phi(\lambda,T)$ for each data set to

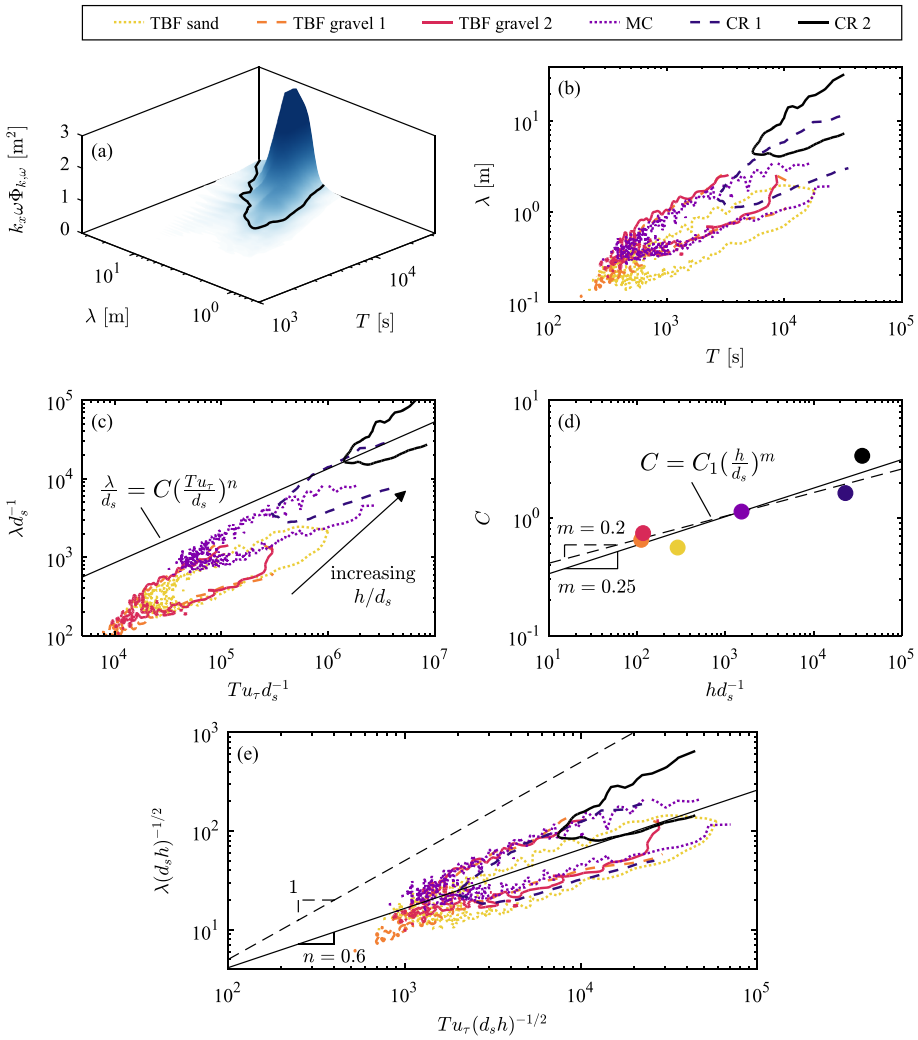

Figure 2. Estimated spatiotemporal bed elevation spectra Φ as functions of wavelength λ and period T. (a) Sample premultiplied spectrum for the CR 2 data set, where the black line is a contour at 5% of the maximum $\Phi_{k,\omega}$. (b) Dimensional spectra showing contours corresponding to 5% of the maximum value for each data set. (c) Spectra contours normalized using frictional scaling parameters, with the h/d_s trend indicated. (d) Values of the intercept C as a function of (h/d_s); the fitted power law exponent is $m = 0.24 \pm 0.13$. (e) Spectra contours normalized using the proposed mixed scaling parameters, with the observed power law coefficient $n = 0.6$ compared to a scale-invariant slope of 1. The legend indicates the Tilting Bed Flume (TBF), Main Channel (MC), and Colorado River (CR) data sets in Table 1.

Equation 1with $n = 0.6$ and the new correction factor, $m = 0.24 \pm 0.13$ was found to minimize the variability of the constant C_1. For simplicity in the resulting mixed scaling, we consider a simplified model for $m = 0.2$, which is within the uncertainty bounds of the fit; it provides the advantage to reduce exactly the two dimensionless scaling parameters into a single frictional scaling one, with a geometrically averaged length scale $(hd_s)^{1/2}$. The updated scaling relationship becomes

$$\frac{\lambda}{d_s} = C_1 \left(\frac{h}{d_s}\right)^{0.2} \left(\frac{Tu_\tau}{d_s}\right)^{0.6}, \tag{2}$$

where $C_1 = 0.26$ was determined by a fit on the whole data set. The terms in Equation 2 can be rearranged such that the correction factor is contained within the normalization of λ and T, leading to

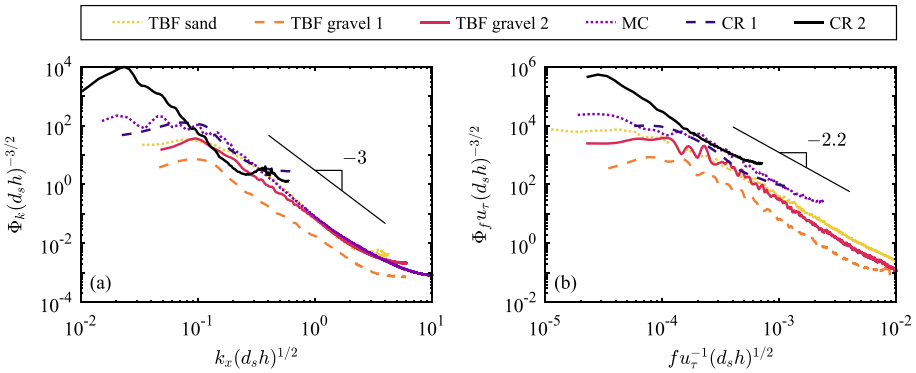

Figure 3. Estimated one-dimensional spectra Φ, normalized using the proposed mixed scaling. (a) Spatial spectra as a function of longitudinal wavenumber k_x. (b) Temporal spectra as a function of frequency f. The legend indicates the Tilting Bed Flume (TBF), Main Channel (MC), and Colorado River (CR) data sets in Table 1.

$$\frac{\lambda}{\sqrt{d_s h}} = C_1 \left(\frac{T u_\tau}{\sqrt{d_s h}} \right)^{0.6}. \tag{3}$$

We acknowledge that using the log-log linear fit $m = 0.24$ yields to length scale exponents $d_s^{(1-w)} h^w$, with $w = m/(1-n)$, thus specifically $d_s^{0.4} h^{0.6}$, as compared to $m = 0.2$ and $\sqrt{d_s h}$. While the contribution of d_s and h in determining the bedform wavelength λ may not be precisely equal as indicated by the simplified $\sqrt{d_s h}$, the important conclusion is that a mixed scaling of d_s and h is required to describe the variability in the bedform wavelength across all the data sets. This mixed scaling is demonstrated in Figure 2e, which shows a reasonable collapse of the data sets. The contour regions corresponding to the range of wavelength and period exhibited by the bedforms align closely for all the data sets, including the Colorado River data with the largest scale separation h/d_s. Similarly for the one-dimensional spectra in Figure 3, the bedform variability is contained within the same range of longitudinal wavenumber, k_x, and frequency, f, when normalized by u_τ and $\sqrt{d_s h}$. Using the updated power law exponent and mixed length scaling, the subsequent bedform convective velocity U_b relationships are derived:

$$\frac{U_b(T)}{u_\tau} = C_1 \left(\frac{T u_\tau}{\sqrt{h d_s}} \right)^{-0.4} \quad \text{and} \quad \frac{U_b(\lambda)}{u_\tau} = C_2 \left(\frac{\lambda}{\sqrt{h d_s}} \right)^{-0.67}, \tag{4}$$

where $C_2 = C_1^{0.33} \approx 0.64$. Note that the normalization of U_b by the shear velocity u_τ results from the normalization of T and it is not prescribed. Equation 4 is also consistent with the expected inverse relationship in which the larger bedforms move slower than the smaller ones.

5. Discussion

We acknowledge here the limitations and some theoretical and practical implications of this work. The proposed model of scale-dependent velocity is strictly valid for uniform flows under the additional key assumption that bedforms develop and migrate under the same hydraulic conditions, implying that both u_τ and h remain invariant as representative scales throughout the process. In natural environments, this is not always verified. As reported in Leary and Buscombe (2020), during the Colorado River 2 case, the discharge decreased over the course of the measurements. The decreasing discharge implies that our local (in time) estimate of the shear velocity underestimates the shear stress that initiated and advected the bedforms under higher discharge conditions at the beginning of the measurement. We infer that the discrepancy in the Colorado River 2 contour observed in Figure 2e) is due to the transient conditions and disequilibrium (Myrow et al., 2018) between the flow and the bathymetry: a higher u_τ would provide a better agreement with the other data sets. A similar discrepancy is not observed in the Colorado River 1 spectrum, even though the discharge was increasing in this case. This is consistent with previous observations of bedform hysteresis: bathymetry evolution is known to quickly adjust to increasing flow rates, while it is more resilient under

decreasing flows, as confirmed by the signature of preserved bedforms in the stratigraphy (Leary & Ganti, 2020; Nicholas et al., 2016; Reesink & Bridge, 2007). It is important to note that the uncertainty in the definition of u_τ and d_s is reflected in the uncertainty of the scaling exponent. In particular, we acknowledge that the estimate of $m = 0.24 \pm 0.13$ is based on a few number of points and that the provided margins of error do not account for the uncertainties of each single realization in the $C,\ hd_s^{-1}$ domain of Figure 2d. Hence, though the dependency on h/d_s and the need for a mixed length scale are conceptually relevant, more experiments are needed to confirm a more precise value for the scaling exponent m.

From a theoretical perspective, the purely frictional formulation of Guala et al. (2014) is corrected with the parameter h/d_s, which is consistent with the granularity term defined by Paola et al. (2009). h/d_s is analogous to the turbulent boundary layer Reynolds number $Re_\tau = \delta u_\tau/\nu$, which is a measure of scale separation in between outer length scale, δ, confining the size of the largest turbulent motions, and the inner (viscous) scale, ν/u_τ, corresponding to the smallest turbulent motions at the (smooth) wall. Similar to how the turbulent motions self-organize into the range of scales between $O(\delta)$ and $O(\nu/u_\tau)$, bedforms are also observed to self-organize in the range of scales between $O(h)$ and $O(d_s)$.

In the simplified mixed scaling model, the explicit formulas for scale-dependent bedform velocity could be used for different purposes. $U_b(T) = 0.26\ u_\tau(Tu_\tau/\sqrt{hd_s})^{-0.4}$, paired with the scale dependent variance of bed elevation (i.e., an estimated frequency spectrum), may provide a reliable estimate of scale-dependent mass flux, which can be integrated to provide the bedform contribution to sediment transport using a single point sensor measuring $z(t)$. $U_b(\lambda) = 0.64\ u_\tau(\lambda/\sqrt{hd_s})^{-0.67}$ may provide a functional relationship between the bedform stratigraphic signature (bedform wavelength and sediment diameter) and the flow (shear velocity and water depth), which could be helpful in paleohydraulic reconstruction studies. More specifically, Ganti et al. (2013) infer that the curvature of the stratigraphic boundaries can be phenomenologically related to the deformation of the bedforms, a portion of which we argue it is associated with their scale-dependent migration, and more precisely to the derivative of the scale-dependent convection velocity $\partial Ub/\partial\lambda$ (in the case limit of rigid translation that would be zero). This opens the possibility to assume a characteristic shape relating the bedform wavelength to its height and to the corresponding water depth (still challenging, see Cisneros et al., 2020) and thereby estimate the shear velocity u_τ as the only unknown term of Equation 4, though with significant uncertainties. Note that both relationships, that is, $U_b(\lambda)$ and $U_b(T)$, imply U_b to scale with u_τ regardless of the bedform size. This is unsurprising as u_τ is a scale-invariant representation of the shear stress at the bed, which mobilizes the sediments and thus contributes directly to bedform advection.

6. Conclusion

Spatiotemporal bed elevation data were analyzed for a straight laboratory flume, intermediate-scale channel, and a river under approximately uniform flow conditions and sediment bed material. By comparing results for sand and gravel sediments, various flow discharges, and an orders-of-magnitude range of channel geometries up to the scale of the Colorado River, unambiguous relationships were determined using spectral analysis to explain the variability of fluvial bathymetry in the frequency and wavenumber domain. First, the results confirmed that bedforms are not rigidly translated at a constant velocity, and smaller bedforms migrate faster than large ones. Accounting for the scale-dependent migration velocity is critical to properly transforming a temporal signal into spatial patterns, estimating the bedform mass flux, and understanding bedform deformation. Second, the channel depth, h, is required in addition to the frictional scaling parameters u_τ and d_s, introduced in Guala et al. (2014), to describe the range of bedform wavelength and period observed among the laboratory- and field-scale channels. The weak dependency on h/d_s accounts for the self-organization scaling range of sediment into bedforms, which suggests an analogy to the outer to inner scale ratio embedded in the Reynolds number. In a further modeling step, the confinement effect of the depth on the evolution of fluvial bedforms has been reasonably approximated by a mixed length scale $\sqrt{hd_s}$ to normalize the bedform length. The findings result in a simple model of scale-dependent bedform migration velocity applicable to the range of wavelengths exhibiting power law behavior in Figure 3. The model was confirmed by the reasonable agreement of spatiotemporal spectra across all data sets, including a range of flows in the upper Colorado River representing a natural fluvial environment.

Acknowledgments

The laboratory data used in this contribution were acquired by Guala et al. (2014) and are available at https://personal.cege.umn.edu/~guala/Michele_datasets.html (Tilting Bed Flume). Main Channel data were collected by Musa et al. (2018) and are available at https://hdl.handle.net/11299/203913. Colorado River data were collected by M. Kaplinski, D. Buscombe, and P. Grams with support from the Glen Canyon Dam adaptive management program administered by the U.S. Department of the Interior Bureau of Reclamation. These data are available at https://doi.org/10.5967/M02J6904 (Leary & Buscombe, 2020) Any use of trade, product, or firm names is for descriptive purposes only and does not imply endorsement by the U.S. Government.

References

Aberle, J., & Nikora, V. I. (2006). Statistical properties of armored gravel bed surfaces. *Water Resources Research*, *42*, W11414. https://doi.org/10.1029/2005WR004674

Ashley, T. C., McElroy, B., Buscombe, D., Grams, P. E., & Kaplinski, M. (2020). Kinematic controls on the geometry of the preserved cross sets. *Journal of Geophysical Research: Earth Surface*, *56*, e2019WR02588. https://doi.org/10.1029/2019WR025883

Best, J. (2005). The fluid dynamics of river dunes: A review and some future research directions. *Journal of Geophysical Research*, *110*, F04S02. https://doi.org/10.1029/2004JF000218

Bradley, R. W., & Venditti, J. G. (2017). Reevaluating dune scaling relations. *Earth-Science Reviews*, *165*, 356–376.

Bradley, R. W., & Venditti, J. G. (2019). The growth of dunes in rivers. *Journal of Geophysical Research: Earth Surface*, *124*, 548–566. https://doi.org/10.1029/2018JF004835

Cisneros, J., Best, J., van Dijk, T., de Almeida, R. P., Amsler, M., Boldt, J., et al. (2020). Dunes in the world's big rivers are characterized by low-angle lee-side slopes and a complex shape. *Nature Geoscience*, *13*, 156–162. https://doi.org/10.1038/s41561-019-0511-7

Coleman, S. E., & Nikora., V. I. (2009). Bed and flow dynamics leading to sediment wave initiation. *Water Resources Research*, *45*, W04402. https://doi.org/10.1029/2007WR006741

Colombini, M., & Stocchino, A. (2012). Three dimensional river bed forms. *Journal of Fluid Mechanics*, *695*, 63–80.

Erm, L. P., & Joubert, P. N. (1991). Low-Reynolds-number turbulent boundary layers. *Journal of Fluid Mechanics*, *230*, 1–44. https://doi.org/10.1017/S0022112091000691

Ganti, V., Paola, C., & Foufoula-Georgiou, E. (2013). Kinematic controls on the geometry of the preserved cross sets. *Journal of Geophysical Research: Earth Surface*, *118*, 1296–1307. https://doi.org/10.1002/jgrf.20094

Ganti, V., Straub, K. M., Foufoula-Georgiou, E., & Paola, C. (2011). Space-time dynamics of depositional systems: Experimental evidence and theoretical modeling of heavy-tailed statistics. *Journal of Geophysical Research*, *116*, F02011. https://doi.org/10.1029/2010JF001893

Guala, M., Singh, A., BadHeartBull, N., & Foufoula-Georgiou, E. (2014). Spectral description of migrating bed forms and sediment transport. *Journal of Geophysical Research: Earth Surface*, *119*, 123–137. https://doi.org/10.1002/2013JF002759

Hino, M. (1968). Equilibrium-range spectra of sand waves formed by flowing water. *Journal of Fluid Mechanics*, *34*(3), 565–573.

IEA (2017). Renewable statistics. International Energy Agency.

Kaplinski, M., Hazel, J. E., Grams, P. E., & Davis, P. A. (2014). Monitoring fine-sediment volume in the Colorado River ecosystem, Arizona—Construction and analysis of digital elevation models (Open-File Report No. 2014-1052). US Geological Survey.

Keylock, C. J., Singh, A., & Foufoula-Georgiou, E. (2014). The complexity of gravel bed river topography examined with gradual wavelet reconstruction. *Journal of Geophysical Research: Earth Surface*, *119*, 682–700. https://doi.org/10.1002/2013JF002999

Khosronejad, A., & Sotiropoulos, F. (2014). Numerical simulation of sand waves in a turbulent open channel flow. *Journal of Fluid Mechanics*, *753*, 150–216.

Krogstad, P. A., Kaspersen, J. H., & Rimestad, S. (1998). Convection velocities in a turbulent boundary layer. *Physics of Fluids*, *10*(4), 949. https://doi.org/10.1063/1.869617

LeHew, J., Guala, M., & McKeon, B. J. (2011). A study of the three-dimensional spectral energy distribution in a zero pressure gradient turbulent boundary layer. *Physics of Fluids*, *51*(4), 997–1012. https://doi.org/10.1007/s00348-011-1117-z

Leary, K. C. P., & Buscombe, D. (2020). Estimating sand bedload in rivers by tracking dunes: A comparison of methods based on bed elevation time-series. *Earth Surface Dynamics*, *8*, 161–172.

Leary, K. C. P., & Ganti, V. (2020). Preserved fluvial cross strata record bedform disequilibrium dynamics. *Geophysical Research Letters*, *47*, e2019GL085910. https://doi.org/10.1029/2019GL085910

Marr, J. D., Gray, J. R., Davis, B. E., Ellis, C., & Johnson, S. (2010). *Large-scale laboratory testing of bedload-monitoring technologies: Overview of the StreamLab06 experiments, in bedload-surrogate monitoring technologies. U.S. Geological Survey Scientific Investigations Report* (Vol. 2010-5091, pp. 266–282).

Martin, R. L., & Jerolmack, D. J. (2011). Origin of hysteresis in bed form response to unsteady flows. *Water Resources Research*, *49*, 1314–1333. https://doi.org/10.1002/wrcr.20093

McElroy, B., & Mohrig, D. (2009). Nature of deformation of sandy bed forms. *Journal of Geophysical Research*, *114*, F00A04. https://doi.org/10.1029/2008JF001220

Musa, M., Hill, C., Sotiropoulos, F., & Guala, M. (2018). Performance and resilience of hydrokinetic turbine arrays under large migrating fluvial bedforms. *Nature Energy*, *3*(10), 839–846.

Myrow, P. M., Jerolmack, D. J., & Perron, J. T. (2018). Bedform disequilibrium. *Journal of Sedimentary Research*, *88*(9), 1096–1113.

Nicholas, A. P., Sambrook, G. H., Amsler, M. L., Ashworth, P. J., Best, J. L., Hardy, R. J., et al. (2016). The role of discharge variability in determining alluvial stratigraphy. *Geology*, *44*(1), 3–6.

Nikora, V. I., & Goring, D. G. (2001). Extended self-similarity in geophysical and geological applications. *Mathematical Geosciences*, *33*(3), 251–271.

Nikora, V. I., Sukhodolov, A. N., & Rowinski, P. M. (1997). Statistical sand wave dynamics in one-directional water flows. *Journal of Fluid Mechanics*, *351*, 17–39.

Paola, C., Straub, K., Mohrig, D., & Reinhardt, L. (2009). The unreasonable effectiveness of stratigraphic and geomorphic experiments. *Earth-science Reviews*, *97*, 1–43.

Passalacqua, P., Porté-Agel, F., Foufoula-Georgiou, E., & Paola, C. (2006). Application of dynamic subgrid-scale concepts from large-eddy simulation to modeling landscape evolution. *Water Resources Research*, *42*, W06D11. https://doi.org/10.1029/2006WR004879

Pelletier, J. D. (1999). The self-organization and scaling relationships of evolving river networks. *Journal of Geophysical Research*, *104*(B4), 7359–7375.

Reesink, A., & Bridge, J. (2007). Influence of superimposed bedforms and flow unsteadiness on formation of cross strata in dunes and unit bars. *Sedimentary Geology*, *202*(1-2), 281–296.

Seminara, G. (2010). Fluvial sedimentary patterns. *Annual Review of Fluid Mechanics*, *42*, 43–66.

Shelley, J., Abraham, D., & McAlpin, T. (2013). Removing systemic bias in bed-load transport measurements in large sand-bed rivers. *Journal of Hydraulic Engineering*, *139*(10), 1107–1111.

Simons, D. B., Richardson, E. V., & Nordin, C. F. (1965). Bedload equation for ripples and dunes. *U.S. Geological Survey Professional Paper*, *462*, 1–9.

Singh, A., Czuba, J., Foufoula-Georgiou, E., Marr, J. D., Hill, C., Johnson, S., et al. (2013). Streamlab collaboratory: Experiments, data sets, and research synthesis. *Water Resources Research*, *49*, 1746–1752. https://doi.org/10.1002/wrcr.20142

Singh, A., Fienberg, K., Jerolmack, D. J., Marr, J., & Foufoula-Georgiou, E. (2009). Experimental evidence for statistical scaling and intermittency in sediment transport rates. *Journal of Geophysical Research*, *114*, F01025. https://doi.org/10.1029/2007JF000963

Singh, A., Lanzoni, S., Wilcock, P. R., & Foufoula-Georgiou, E. (2011). Multi-scale statistical characterization of migrating bedforms in gravel and sand-bed rivers. *Water Resources Research*, *47*, WR12526. https://doi.org/10.1029/2010WR010122

Singh, A., Porté-Agel, F., & Foufoula-Georgiou, E. (2010). On the influence of gravel bed dynamics on velocity power spectra. *Water Resources Research*, *46*, WR04509. https://doi.org/10.1029/2009WR008190

Southard, J. B. (1991). Experimental determination of bed-form stability. *Annual Review of Earth and Planetary Sciences*, *19*, 423–455.

Venditti, J. G., Church, M., & Bennett, S. J. (2005). Morphodynamics of small-scale superimposed sand waves over migrating dune bed forms. *Water Resources Research*, *41*, W10423. https://doi.org/10.1029/2004WR003461

Wilcock, P. R., Orr, C. H., & Marr, J. D. (2008). The need for full-scale experiments in river science. *Eos, Transactions American Geophysical Union*, *89*(1), 6–6.

Witt, A., Smith, B. T., Tsakiris, A., Papanicolaou, T., Lee, K., & Stewart, K. S. (2017). Exemplary design envelope specification for standard modular hydropower technology. Oak Ridge National Laboratory, ORNL/TM-2016/298 (pp. 1–143). https://doi.org/10.2172/1343525